SANDIA REPORT

SAND2010-6309
Unlimited Release
Printed September, 2010

A Computational Study of Nodal-Based Tetrahedral Element Behavior

Arne Gullerud

Prepared by
Sandia National Laboratories
Albuquerque, New Mexico 87185 and Livermore, California 94550

Sandia National Laboratories is a multi-program laboratory managed and operated by Sandia Corporation, a wholly owned subsidiary of Lockheed Martin Corporation, for the U.S. Department of Energy's National Nuclear Security Administration under contract DE-AC04-94AL85000.

Approved for public release; further dissemination unlimited.

Sandia National Laboratories

Issued by Sandia National Laboratories, operated for the United States Department of Energy by Sandia Corporation.

NOTICE: This report was prepared as an account of work sponsored by an agency of the United States Government. Neither the United States Government, nor any agency thereof, nor any of their employees, nor any of their contractors, subcontractors, or their employees, make any warranty, express or implied, or assume any legal liability or responsibility for the accuracy, completeness, or usefulness of any information, apparatus, product, or process disclosed, or represent that its use would not infringe privately owned rights. Reference herein to any specific commercial product, process, or service by trade name, trademark, manufacturer, or otherwise, does not necessarily constitute or imply its endorsement, recommendation, or favoring by the United States Government, any agency thereof, or any of their contractors or subcontractors. The views and opinions expressed herein do not necessarily state or reflect those of the United States Government, any agency thereof, or any of their contractors.

Printed in the United States of America. This report has been reproduced directly from the best available copy.

Available to DOE and DOE contractors from
U.S. Department of Energy
Office of Scientific and Technical Information
P.O. Box 62
Oak Ridge, TN 37831

Telephone: (865) 576-8401
Facsimile: (865) 576-5728
E-Mail: reports@adonis.osti.gov
Online ordering: http://www.osti.gov/bridge

Available to the public from
U.S. Department of Commerce
National Technical Information Service
5285 Port Royal Rd
Springfield, VA 22161

Telephone: (800) 553-6847
Facsimile: (703) 605-6900
E-Mail: orders@ntis.fedworld.gov
Online ordering: http://www.ntis.gov/help/ordermethods.asp?loc=7-4-0#online

SAND2010-6309
Unlimited Release
Printed September, 2010

A Computational Study of Nodal-Based Tetrahedral Element Behavior

Arne S. Gullerud
Computational Structural Mechanics and Applications
Sandia National Laboratories
P.O. Box 5800
Albuquerque, NM 87185-1185

Abstract

This report explores the behavior of nodal-based tetrahedral elements on six sample problems, and compares their solution to that of a corresponding hexahedral mesh. The problems demonstrate that while certain aspects of the solution f eld for the nodal-based tetrahedrons provide good quality results, the pressure f eld tends to be of poor quality. Results appear to be strongly affected by the connectivity of the tetrahedral elements. Simulations that rely on the pressure f eld, such as those which use material models that are dependent on the pressure (e.g. equation-of-state models), can generate erroneous results. Remeshing can also be strongly affected by these issues. The nodal-based tet elements as they currently stand need to be used with caution to ensure that their numerical def ciencies do not adversely affect critical values of interest.

Acknowledgment

Many Sandians have given me valuable advice on these simulations and have reviewed these results. Specif c thanks go to Bill Scherzinger, Jake Ostien, Martin Heinstein, and the Sierra Solid Mechanics team for their consideration of this information and willingness to discuss the ramif - cations.

Contents

Summary **9**

1 Introduction **11**

2 Exploratory Analyses **15**

Patch Test 16

Cook's Membrane 17

Beam Bending 21

Taylor Bar Impact 21

Elastic Shear 23

Torsional Cylinder 36

3 Conclusions **43**

References **45**

List of Figures

1.1 Penetration analysis using nodal-based tets with remeshing. Simulation uses simple elastic-plastic models with a constant bulk modulus, however, instead of including an equation-of-state to model bulk stiffening under high velocity impact. . . 13

2.1 Example of a smooth loading curve used to generate a quasi-static response in Presto. Equation for the increasing portion of the curve is $0.001(cos(\pi(t/T - 1)) + 1)/2$, where t is time and $T = 0.002$ is the time at max load. 16

2.2 Meshes for the patch test problems. 17

2.3 Results of patch test analysis. Results from hexahedral (all seven elements) and Nodal-Based Tetrahedral (all 16 nodes) are plotted on top of each other. Top curves are for the xx, yy, and zz terms, while the shear terms are the lower curves. 18

2.4 Equivalent plastic strain for Cook membrane problem, hexes and nodal-based tets. 19

2.5 Pressure for Cook membrane problem, hexes and nodal-based tets. 20

2.6 Stress f uctuation near f xed end of beam for nodal-based tet mesh. 22

2.7 Pressure solution for Taylor impact using a hex mesh. 24

2.8 Pressure solution for Taylor impact using a nodal-based tet mesh. 24

2.9 Diagram of elastic shear problem. 25

2.10 Pressure prof les for elastic shear problem with regularly meshed hexes. Pressure prof les in each picture cover the minimum and maximum range of pressures in the analysis. 26

2.11 Pressure prof les for elastic shear problem with paved hex meshes. Pressure prof les in each picture cover the minimum and maximum range of pressures in the analysis. 27

2.12 Pressure prof les for elastic shear problem with nodal-based tets created from hex meshes. Pressure prof les in each picture cover the minimum and maximum range of pressures in the analysis. Note the ever-increasing range of pressures, which are both positive and negative. 29

2.13 Pressure profiles for elastic shear problem with nodal-based tets created from hex meshes. Pressure profiles in each picture cover from 1e4 to -1e4. Nodes that are adjacent on the mesh may have opposite signs, even in the refined mesh. 30

2.14 Pressures and uneven deformation of inner radius on fine mesh for nodal-based tet solution, $\alpha = 0.005$ and $\beta = 0.01$. 31

2.15 Pressure solutions for coarse nodal-based tetrahedral mesh for various values of α and β. 32

2.16 Pressure solution for front and back of coarse nodal-based tetrahedral mesh with $\alpha = 0.01$ and $\beta = 0.6$. 33

2.17 Stress components for nodal solution of coarse mesh. 34

2.18 Stress components for nodal solution of coarse mesh. 35

2.19 Pressures in torsional cylinder using a hex mesh. 37

2.20 Pressures in torsional cylinder using a nodal-based tet mesh generated from corresponding hex mesh. 38

2.21 Pressures in torsional cylinder using a paved nodal-based tet mesh. 39

2.22 Pressures on exterior/interior of finest nodal-based tet mesh. 40

2.23 Pressures in torsional cylinder using a cross-triangle nodal-based tet mesh (24 tets per hex). 41

2.24 Pressures through center of cylinder with cross-triangle mesh, with standard and nodal-based tets. 42

List of Tables

2.1 Beam bending results 21

2.2 Johnson-Cook material properties used for copper 22

2.3 Final Deformations of Rod, Experimental and Computed 23

Summary

This report explores the behavior of nodal-based tetrahedral (tet) elements on a number of problems in solid mechanics. Nodal-based tet elements modify the standard four-node tet element by volume averaging the element gradient operators at the nodes to permit consitutive evaluations at the nodes. This has been shown to alleviate locking problems seen on the standard four node tet. This element has been implemented within the Sierra Solid Mechanics (Sierra/SM) module, and is used primarily in explicit transient-dynamics. Sierra/SM exploits the fact that the elements are nodally-integrated to facilitate an innovative remeshing scheme that reduces material remapping error by preserving node (and thus integration point) locations. These features make the nodal-based tet with rememshing an attractive technology for lagrangian shock-physics computations, where remeshing can be used to handle very large deformations while reducing the need to remap the state variables of complex material models.

This report presents six sample analyses to explore the response of the nodal-based tet: the patch test, Cook's membrane, beam bending, Taylor bar impact, elastic shear, and a torsional cylinder. These analyses show that the nodal-based tet element provides good quality global metrics in some cases. However, the pressure solution in general is of poor quality, especially in cases with signif cant shear. The pressure f elds generally show high levels of spurious variation between adjoining nodes. Mesh ref nement does not help signif cantly in this variation, nor does modif cation of the element stabilization parameters. The results seem to indicate that the primary driver of the variation in pressures is the connectivity of the mesh; changes in the number of tets that contribute to a node or changes in the orientation of diagonals in a mesh appear to correlate well to the pressure variations.

These results indicate that the nodal-based tet must be used with signif cant caution. They may function well for simulations that do not have signif cant shear and which are dominated by plastic deformation. However, for general use, answers should be inspected carefully before the results are used. The nodal-based tets should probably be avoided if the material model depends on the pressure response. Furthermore, remeshing should be used with caution as well, since the pressure f uctuations are dependent on connectivity, and connectivity can change signif cantly during the remeshing process. More work is needed to understand this phenomenon and to look for ways of alleviating its effects.

Chapter 1

Introduction

The search for an effective tetrahedral (tet) element for solid mechanics has been the source for a signif cant amount of research over the past few decades. The most successful and widely used elements for solid mechanics are typically hexahedral (hex) elements. These elements generally provide good quality results for the comparative computational cost. It can be challenging to mesh arbitrary volumes using hex elements, however; a large portion of a typical analysis task can be spent in creating the original mesh. Tet elements offer signif cant advantages in mesh creation. Because of the simplicity of their geometry, automated tet meshing is more achievable, and thus can signf cantly reduce the overall time spent in analysis. Automated tet meshing can also enable dynamic remeshing in the code, where a new mesh can be created on the f y to improve badly deformed elements.

Despite the advantages that tets provide for meshing, they are not as widely used in solid mechanics because of the quality of results they produce. Standard linear tet formulations are subject to a range of locking phenomenon, causing their response to be quite stiff. To achieve a solution with similar accuracy for a standard hex element, many more tets are typically needed, and it may not be possible to achieve any reasonable answer in the incompressible regime for some meshes [6].

To alleviate the locking issues of the standard four-node tet element, Dohrmann et al. [4] proposed a modif ed formulation which volume averages the gradient operators of the elements connected to each node, enabling all element computations to be done at the nodes instead of the elements. This formulation is referred to as a “node-based” tetrahedron. Several simple examples in their paper demonstrated that the modif cation reduced the locking problems and dramatically improved results. This approach was expanded by Puso and Solberg [10] to include a stabilization term to eliminate zero-energy modes. This stabilization utilized elastic computations on the original elements, of which a small portion were included in the full stiffness of the system. The elastic computations were made to have a similar stiffness to the nodal solution, but the Poissons ratio was limited to keep the elements from approaching incompressibility. An alternative stabilization was proposed by Gee et al. [5] which computes full material response at the elements, and uses only the isochoric part of the response as a stabilization term.

The nodal-based tet element has been implemented at Sandia National Labs in the Sierra Solid Mechanics (Sierra/SM) module, primarily for explicit transient-dynamics simulations [12]. This implementation uses a third approach for stabilization. The elements compute a full material re-

sponse, and both the volumetric and isochoric terms are used for stabilization, but with separate terms to adjust how much is used (α and β for the volumetric and isochoric terms, respectively). By default, these terms are set to $\alpha = 0.01$ and $\beta = 0.35$, which has been shown to work well for bending problems.

Besides the alleviation of locking issues, the nodal-based formation has other advantages. Automated remeshing can greatly extend the level of deformation permitted in a lagrangian f nite element formulation by reconstructing the mesh to replace elements with bad aspect ratios, then remapping the element values to the new mesh. This process of remapping is very tricky for the material state variables of complex materials since the collection of state variables represent a consistent material state. Mapping each of the state variables independently can result in an inconsistent material state, resulting in signif cant error. Proper approaches to do this are the subject of current research at Sandia and elsewhere. In the case of the nodal-based tet, the consitutive evaluations for the nodal-based tets are done at the nodes, thus the material state variables exist at the nodes. It is then possible to create a remeshing technique that seeks to preserve nodal locations, re-def ning the elements that connect them as needed to eliminate excessively deformed elements. This eliminates much of the need to remap the material state variables, thus may signif cantly reduce the error incurred by remeshing. Such a technique has been implemented within Sierra/SM, and has been used for a range of very large deformation analyses([2], [3], [1]).

An example of the use of the remeshing technique is shown in Figure 1.1. In this example, a titanium rod impacts a steel disk at 4 km/sec. The remeshing technique is able to model severe deformations as well as material breakup, and includes an automated ref nement mechanism to better capture surfaces created during the impact. The material models used for this analysis were simple elastic-plastic models with a constant bulk modulus.

To properly model the bulk response of these materials at this impact velocity, equation-of-state (EOS) models are preferred. These models couple the bulk response of the material with the internal energy caused by the deformation, leading to a stiffening of the bulk modulus and the ability to capture the formation of shock waves. For problems where impact velocities are a signif cant portion of the bulk sound speed, EOS models are needed for accurate modeling. If the nodal-based tet coupled with remeshing is able to function properly with EOS models, then the capabilities within Sierra/SM represent a signif cant new numerical approach for computing simulations within the shock-regime. In order for an element to use an EOS model, however, it must be able to capture pressure f eld response effectively.

The purpose of this report is to explore the ability of the nodal-based tet to properly capture the pressure f eld using simple example problems. Six sample analyses are used to assess the element. The analyses are as follows:

- Patch test: this cannonical problem tests whether the element can capture constant stress/strain f elds
- Cook's Membrane: a tapered bar under a mild tip loading
- Beam Bending: a thin beam under applied pressure

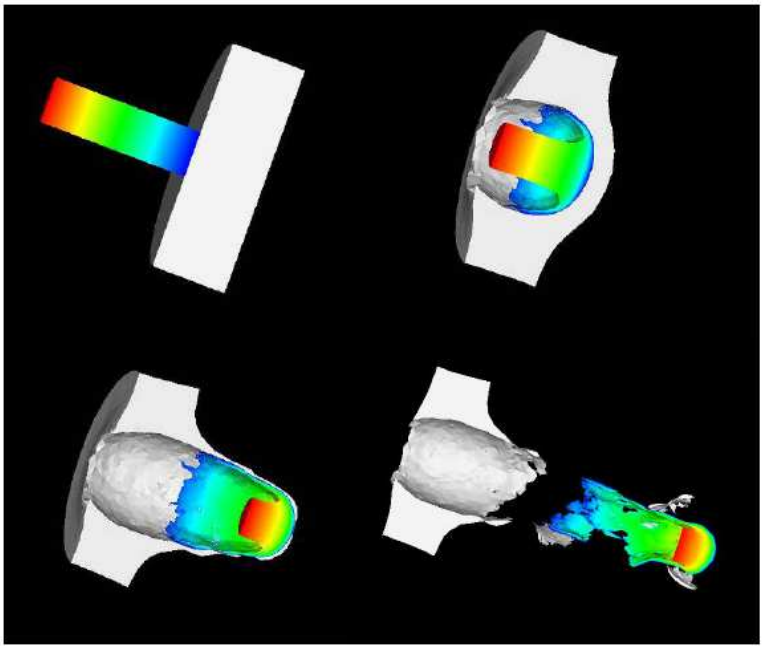

Figure 1.1. Penetration analysis using nodal-based tets with remeshing. Simulation uses simple elastic-plastic models with a constant bulk modulus, however, instead of including an equation-of-state to model bulk stiffening under high velocity impact.

- Taylor Bar Impact: a copper rod impacting a rigid plate
- Elastic Shear: an annulus of elastic material f xed on the outer radius with a rotation of the inner radius
- Torsion Cylinder: a cylinder subjected to a torsional loading

In each of these cases, the problems are modeled using nodal-based tet elements as well as hex elements. The solutions are compared against each other and expected results. Of particular interest is the behavior of the pressure f eld, which is critical for the use of EOS models and other pressure-dependent constitutive models. In most of the analyses, a quasi-static-like loading is used along with elastic material models to simplify the assessment of the solutions.

The remainder of the report contains the description of each of the example problems and the results for both hex and nodal-based tet elements, plus an assessment of the quality of the solutions. This is then followed by conclusions from the analyses.

Chapter 2

Exploratory Analyses

In order to assess the qualities of the nodal-based tetrahedron (tet), this report examines the performance of this element on a collection of six example problems. Of particular interest is the quality of the pressure f eld solution. This metric is chosen in order to assess the applicability of nodal-based tets for pressure-dependent material models, such as equations-of-state. In each case, the nodal-based tet results are compared against the response of the standard uniform-gradient hexahedron and against expected results. All of the simulations were performed using the Sierra Solid Mechanics (Sierra/SM) explicit transient-dynamics capability, which is also called Presto [12]. The version used was 4.16, which was released in Spring of 2010. Despite the fact that an explicit code was used for the simulations, all of the problems apart from the Taylor bar impact employed a smooth loading that approximates a quasi-static response (see Fig 2.1 for an example). Most of the problems also utilized smooth elastic material response in order to simplify the assessment of the element results. For the nodal-based tets, reported results are typically nodal values. A small portion of the element values are used to stabilize the nodal solution. Unless otherwise stated, the default stabilization terms were used ($\alpha = 0.01$, $\beta = 0.35$).

The f rst four example problems include the patch test, Cook's membrane, beam bending, and Taylor bar impact. The nodal-based tet generally shows good global response for these problems, however in the beam bending and Taylor bar impact tests the pressure f elds are not as clean and smooth as expected. The f nal two tests show signif cant def ciencies with the element under loading conf gurations that have signif cant shear deformation. The def ciencies do not appear to go away with mesh ref nement. These tests are the rotational shearing of an elastic annulus and a torsional loading on a cylinder. Signif cant spurious variation of the pressure f eld is evident on these problems. The spurious behavior appears to be fundamentally related to the connectivity of the tetrahedral meshes; nodal-based meshes without a very regular structure show stress concentrations, whereas tetrahedral meshes with a very structured shape ("cross-triangle" mesh, with 24 tets per hex) show signif cantly better solution quality.

The analyses covered in this section are:

- Patch test
- Cook's Membrane
- Beam Bending

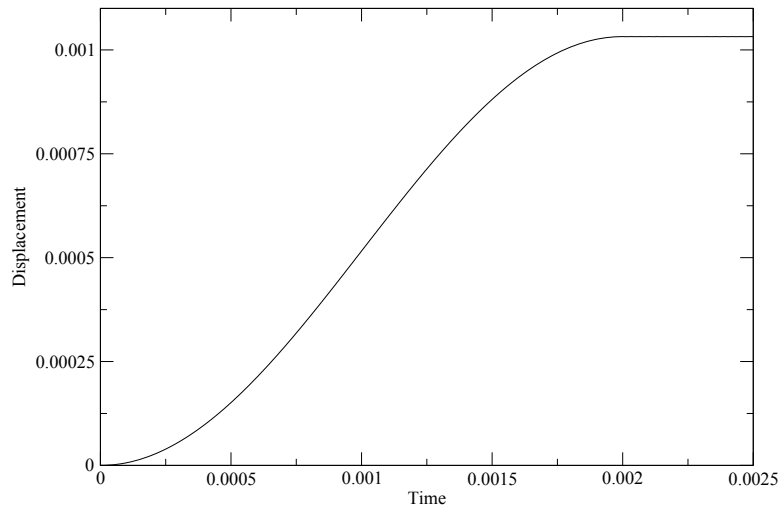

Figure 2.1. Example of a smooth loading curve used to generate a quasi-static response in Presto. Equation for the increasing portion of the curve is $0.001(cos(\pi(t/T-1))+1)/2$, where t is time and $T = 0.002$ is the time at max load.

- Taylor Bar Impact
- Elastic Shear
- Torsion Cylinder

Patch Test

The patch test [7] is a standard test for element quality widely used in the literature. For hexahedral elements in 3D, the patch test takes the form of a seven element mesh f tting into a cube, where a single element inside the cube is distorted such that none of it's sides are co-planar with cube sides, and the other six elements connect the faces of the distorted element to the faces of the cube. A displacement loading is applied on the outside of the cube such that there is a constant strain in all six components of the strain tensor, leading to a constant stress in all six components of the stress tensor. This test demonstrates that the element is linearly consistent. The material model is elastic, and the loading follows the smooth loading in Figure 2.1. The displacements and material constants are chosen such that σ_{xx}, σ_{yy}, and σ_{zz} should be 4000, while σ_{xy}, σ_{yz}, and σ_{zx} should be 800.

Figure 2.2 shows the patch test mesh for the hexahedral and nodal-based tetrahedral elements. The tetrahedral patch test mesh is generated from the hexahedral mesh using six tetrahedral elements per hexahedral element for a total of 42 elements; no additional nodes are required for this new mesh. Figure 2.3 shows the stresses for all the hex elements and all of the nodal stresses

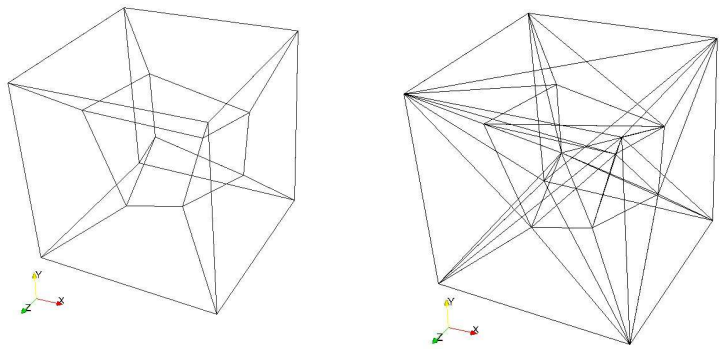

(a) Hexahedral Mesh **(b)** Tetrahedral Mesh

Figure 2.2. Meshes for the patch test problems.

from the nodal-based tets plotted on top of each other. In both cases, the expected stresses are reached and are the same for all stress points. This indicates that both elements pass the patch test and are thus linearly consistent. Note also that the smooth loading produces no readily observable oscillation, thus reasonably approximates a quasi-static solution.

Cook's Membrane

The Cook's Membrane problem is a standard analysis used for code verif cation and for the assessment of element behavior. The problem consists of a tapered panel in plane strain with a shear load applied to the end. Puso and Solberg [10] report results for this analysis using their implementation of the nodal-based tet, thus this test serves as a comparison of their implementation with the one available in Sierra/SM. The panel is 48 units long, 44 units high at the support and 16 units high at the end. The material model used is elastic-plastic with a Young's modulus of 70, Poisson's ratio of 0.333, a yield stress of 0.243, and a linear hardening modulus of 0.15. The total shear load was 1.8 applied as a smooth function (see Figure 2.1), which produced a slight bending displacement over the length. The problem was modeled using both hex elements and nodal-based tet elements (converted from the hex mesh). The hex mesh used 53 elements along the length and 23 elements along the height; the tetrahedral mesh converted each hex into 6 tets. The nodal-based tet simulation used the default α and β parameters (0.01 and 0.35, respectively).

The resulting equivalent plastic strain contours are shown in Figure 2.4, and the corresponding pressure contours are shown in Figure 2.5. For both quantities of interest, the solution from the

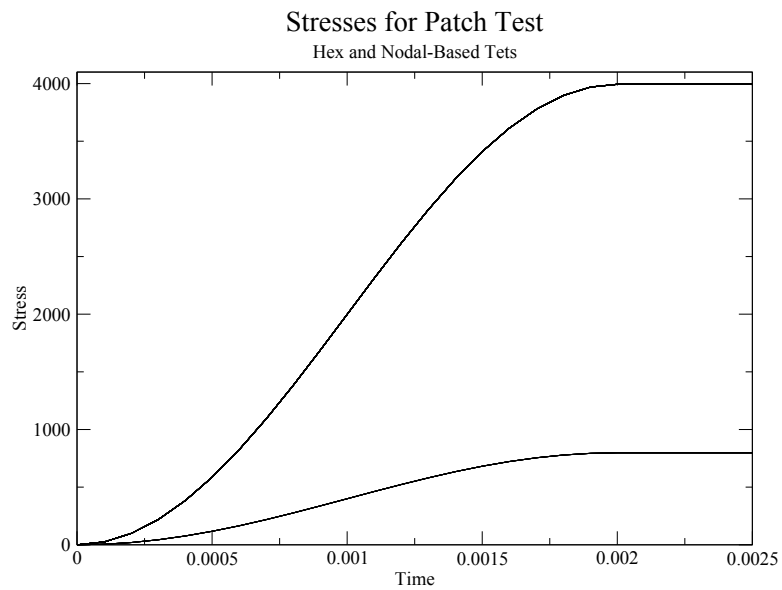

Figure 2.3. Results of patch test analysis. Results from hexahedral (all seven elements) and Nodal-Based Tetrahedral (all 16 nodes) are plotted on top of each other. Top curves are for the xx, yy, and zz terms, while the shear terms are the lower curves.

nodes for the nodal-based tet mesh and the solution from elements of the hex mesh are qualitatively the same. They also compare well with the solutions published in Puso and Solberg [10]. Additionally, both f gures show the solution of the nodes and of the elements for the nodal-based tetrahedrons. Note again that the nodal values are the values of interest; the element values are used purely as a stabilization term weighted into the nodal results.

In the case of the equivalent plastic strains, the node and element values are very similar. However, the nodal and element pressures are very different – the nodal values show a smooth variation over the model, while the element pressures show signif cant oscillation of pressures and different values in some locations. This illustrates a general issue about the stabilization strategy used in the Sierra/SM implementation of the nodal-based tets. Because a very small percentage of the element solution is used in the full nodal-based tet solution, the element solution can drift signif cantly from the overall solution. This must be kept in mind when using the nodal-based elements; the values from the element stabilization may not be reasonable. This may also suggest that the stabilization proposed by Puso (using a purely elastic model at the elements instead of the same consitutive model as the nodes use) may be more appropriate.

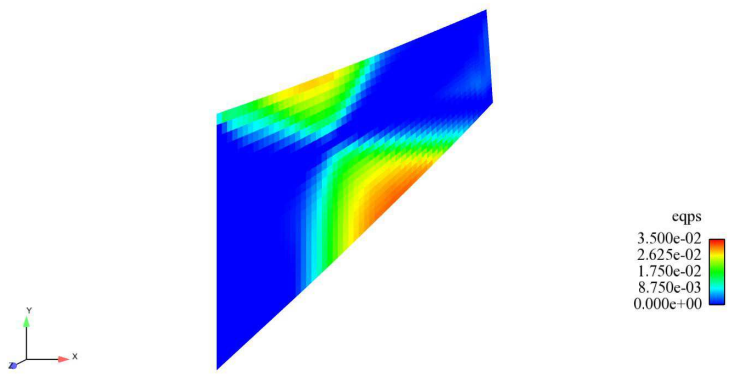

(a) Hexahedron Solution

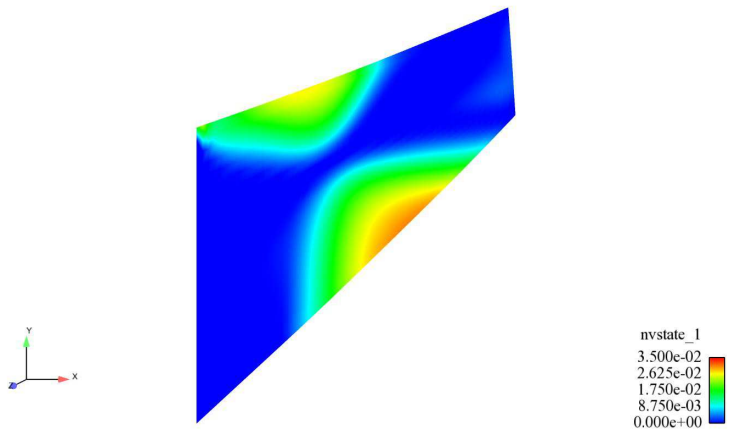

(b) Nodal-Based Tetrahedron Solution: nodes

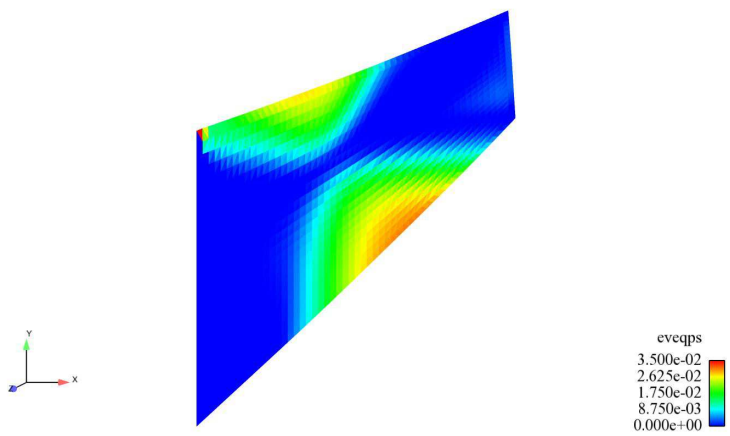

(c) Nodal-Based Tetrahedron Solution: elements

Figure 2.4. Equivalent plastic strain for Cook membrane problem, hexes and nodal-based tets.

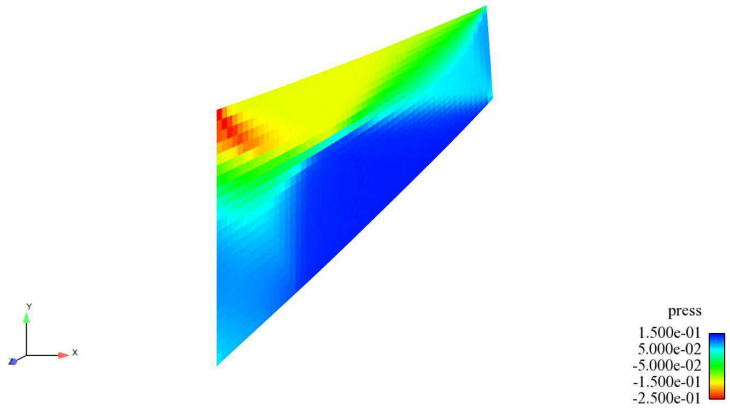

(a) Hexahedron Solution

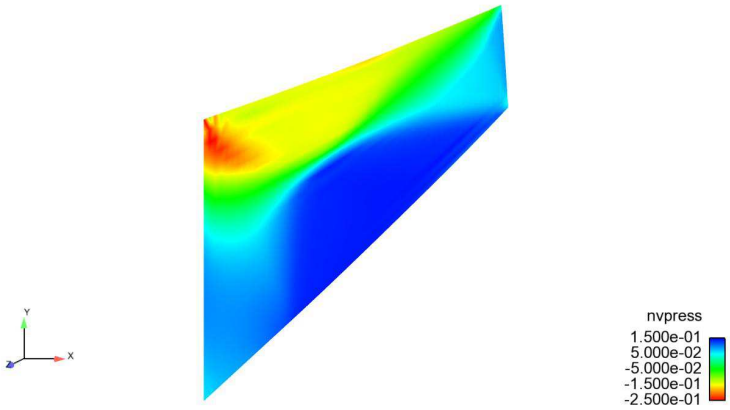

(b) Nodal-Based Tetrahedron Solution: nodes

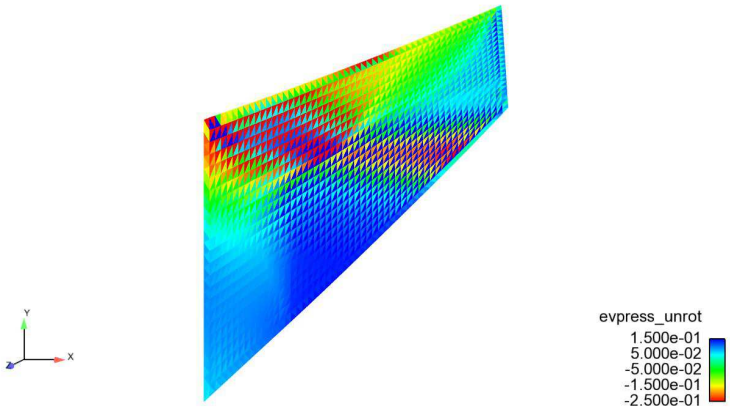

(c) Nodal-Based Tetrahedron Solution: elements

Figure 2.5. Pressure for Cook membrane problem, hexes and nodal-based tets.

Beam Bending

Another example to explore the performance of the nodal-based tet is a beam bending problm. The beam is constrained on one end, with a pressure load across the top. The beam is 10 inches long, 2 inches deep, and 1 inch high. The material is elastic, with Youngs modulus of 1.0e6 and Poissons ratio of 0.3. The pressure load is distributed over the entire top surface with a magnitude of 400. The solution is computed using hex, standard tetrahedrons, and nodal-based tetrahedrons (with stabilization parameters $\alpha = 0.01$ and $\beta = 0.35$), each with 3 elements through the thickness. The nodal-based tet mesh is generated from the hex mesh, with 6 tets per hex. The pressure is increased using a smooth loading function (like Figure 2.1) in order to achieve a quasi-static-like loading. Table 2.1 shows the computed solutions compared to the theoretical solution. The nodal-based tet solution is closest to the expected value, while the standard tet is signif cantly different. Previous work has demonstrated that the nodal-based tet provides very good quality results under additional mesh ref nement [9].

Table 2.1. Beam bending results

Result Source	Tip Displacement
Beam Theory	0.60
Standard tet	0.41
Hex	0.64
Nodal-based tet	0.61

A closer look at the pressures in the nodal-based tet case, however, show that there is some anomolous behavior where the stresses are highest – at the f xed boundary condition. Figure 2.6 shows the pressures at the f xed end of the beam and the stresses along the top and bottom of the beam. A non-smooth f uctuation is evident along the top of the beam. Even though the global displacement results look good, there are variations in pressure near the boundary condition that are not seen in the hex mesh and which appear to be related to the numerics of the nodal-based tets.

Taylor Bar Impact

The Taylor bar impact experiment is frequently used to explore the behavior of material under various loading rate conditions with substantial plastic deformation. In this test, a cylinder of material is propelled at a specif ed initial velocity and impacts a stiff surface. A large amount of experimental data is available for a range of velocities on a variety of materials. Here, we choose a cylinder 25.4 mm in length and 7.6 mm in diameter made of copper with an initial velocity of 190 m/s. The Johnson Cook model is used to model the copper, with values given in table 2.2. Note that this velocity is slow enough that bulk strengthening is negligable, and thus an equation-of-state is not needed to model the response effectively.

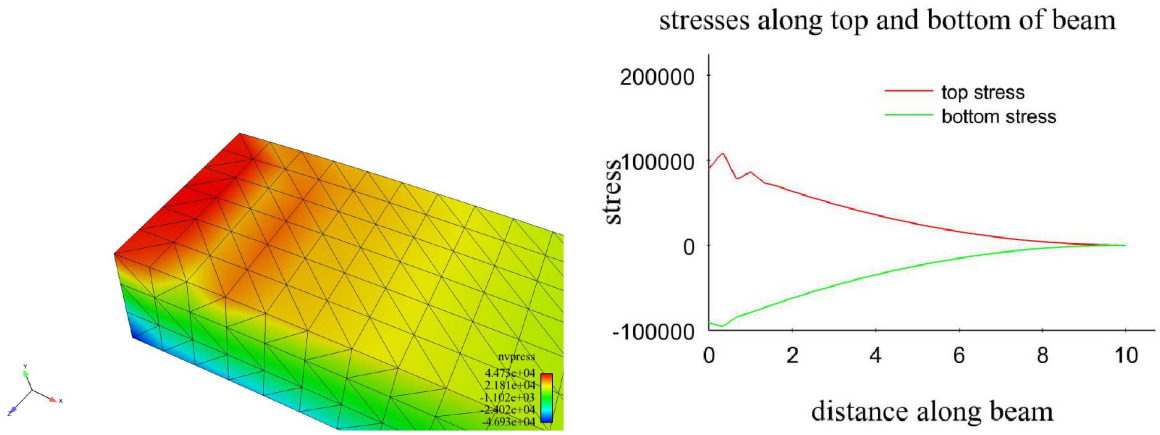

(a) Pressure contours near f xed boundary

(b) σ_{xx} plotted along length of bar

Figure 2.6. Stress f uctuation near f xed end of beam for nodal-based tet mesh.

Table 2.2. Johnson-Cook material properties used for copper

Property	Value
Density	8960.0 kg/m^3
Youngs modulus	124.0 GPa
Poissons ratio	0.34
Reference temperature	295.0 K
Melt temperature	1356.0 K
Yield stress	90.0 MPa
Hardening constant	292.0 MPa
Hardening exponent	0.31
Rate constant	0.025
Thermal exponent	1.09

Table 2.3. Final Deformations of Rod, Experimental and Computed

Result Source	Final Length (mm)	Final Base Diameter (mm)
experiment	17.2	14.6
hex	17.0	14.1
nb tet ($\alpha = 0.01, \beta = 0.35$)	17.0	14.2
nb tet ($\alpha = 0.00, \beta = 0.00$)	17.0	14.6
nb tet ($\alpha = 0.00, \beta = 0.25$)	17.0	14.4
nb tet ($\alpha = 0.25, \beta = 0.00$)	17.0	13.3
nb tet ($\alpha = 0.25, \beta = 0.25$)	17.0	13.2

The cylinder was meshed with both hex elements and nodal-based tetrahedral elements. For the hex mesh, roughly 30 elements were used along the length and 20 through the diameter. The nodal-based tet mesh was constructed from the hex mesh with 6 tets used per hex. After impact, the f nal bar length and f nal base diameter were computed and compared to published experimental results. Several pairs of stabilization parameters (α and β) were used for the nodal-based tet runs to explore the sensitivity of the f nal answer to these values. The results are shown in Table 2.3. The results show good agreement in the f nal length with all analyses, and generally good agreement in the f nal base diameter, though signif cant variability was possible with different α and β pairs. From these global metrics, the nodal-based tet appears to perform very well in this situation, and provides results that are as good or better than those of the standard hex element.

The quality of the nodal-based solution is not as good when we investigate the pressure f elds in the simulation, however. Figure 2.7 shows the pressure f elds for the hex mesh on the interior and exterior of the body. Both the full pressure range and a more limited pressure range are shown in the f gure. These results show a compressive pressure in the core near the bottom, with tensile pressure on the outside of the same region. The limited pressure range shows clearly where the pressures are positive and negative, showing a generally symmetric result with sharp transitions between sign. Figure 2.8 shows the same pressure plots for the nodal pressures for the nodal-based tet. In this case, the solutions are not as smooth. The full pressure ranges are an order of magnitude higher for the nodal-based tet compared to the hex. In the plots with the reduced pressure range, the results show signif cant speckling, where adjacent nodes may have positive and negative pressures. The transition between positive and negative pressure is not smooth at all. Although there are no experimenal results that indicate what the pressures actually are, the nodal-based results do not look as physically reasonable as the hex solution.

Elastic Shear

The next problem explores the behavior of the nodal-based element under a fairly severe shear loading. The elastic shear problem is an annulus which is f xed on the outside radius and is sub-

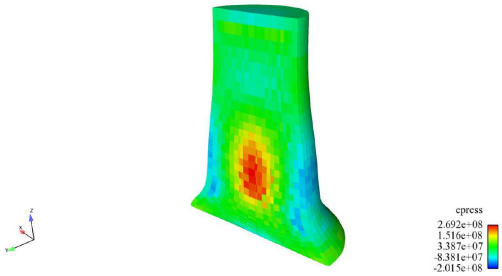

(a) Interior pressures, full pressure range.

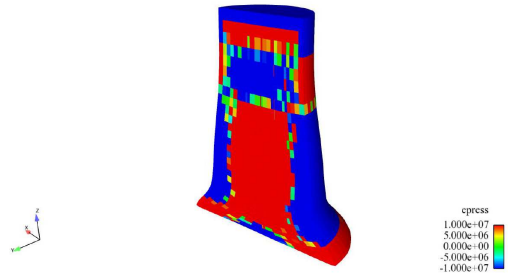

(b) Interior pressures, reduced pressure range.

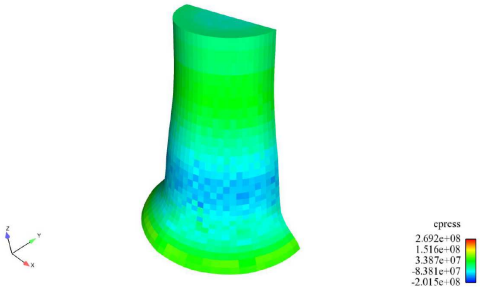

(c) Exterior pressures, full pressure range.

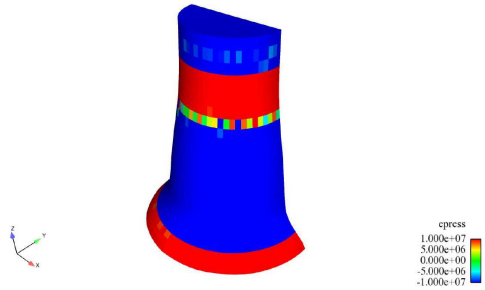

(d) Exterior pressures, reduced pressure range.

Figure 2.7. Pressure solution for Taylor impact using a hex mesh.

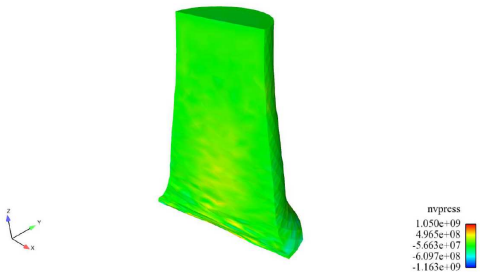

(a) Interior pressures, full pressure range.

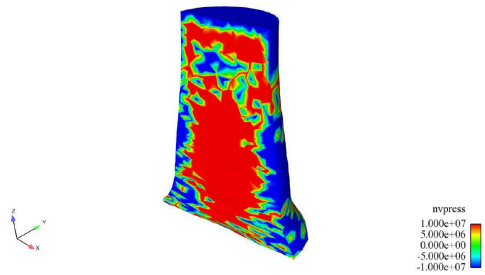

(b) Interior pressures, reduced pressure range.

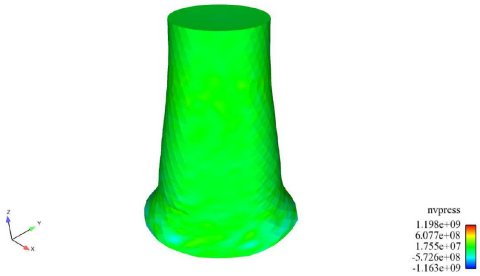

(c) Exterior pressures, full pressure range.

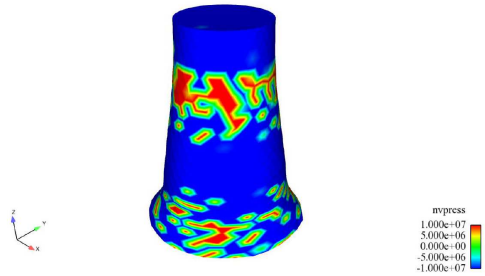

(d) Exterior pressures, reduced pressure range.

Figure 2.8. Pressure solution for Taylor impact using a nodal-based tet mesh.

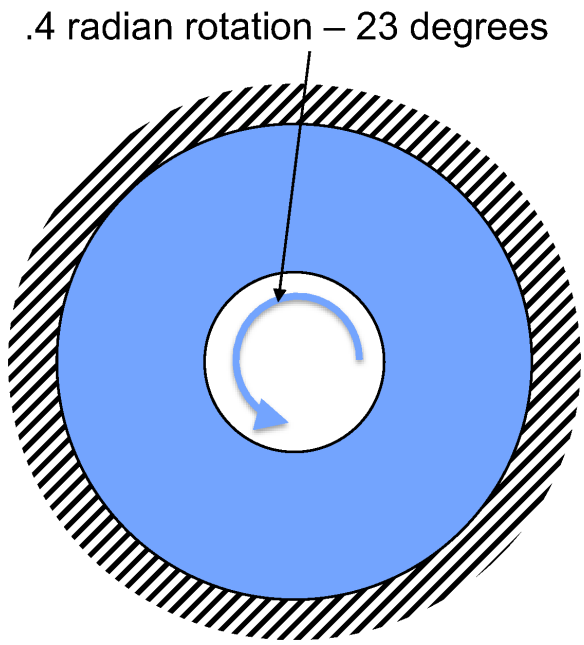

Figure 2.9. Diagram of elastic shear problem.

jected to an internal rotation of the inner radius of 0.4 radians (see Figure 2.9). The material model is elastic with a bulk modulus of 1.542e6 and a Poisson's ratio of 0.2. On the inner radius, the rotation is applied in a smooth ramp loading as shown in Figure 2.1, and no constraints are applied in the radial direction. Analyses using both hexahedral and nodal-based tetrahedral elements were conducted. For both element types, three levels of mesh ref nement were run, with 7, 13, and 28 elements in the radial direction, and 1, 3, and 6 elements through the thickness. The hex meshes included a regular mesh as well as a paved mesh, while the nodal-based tetrahedral meshes were converted from the regular hex mesh using 6 tets per hex. The problem was held in plane strain in the thickness direction. As in the case of the previous problem, the primary metric of interest in these analyses is the pressure f eld.

Figures 2.10 and 2.11 show the solution of the pressure f eld using hexahedral elements. The f rst set of contours show the solution with three levels of mesh ref nement with a regular mesh while the second show the paved mesh results. In the regularly meshed case, the solution is always symmetric and smooth. In the paved mesh case, the coarsest mesh appears to have a signif cant range of variability in the pressure solution near the inner radius. However, with mesh ref nement, the solution looks more and more regular. The pressure range for the f nest regular and paved meshes is very similar: the pressures range from 1.31e+4 to 1.03e+5 for the regular mesh and 1.30e+4 to 1.06e+5 for the paved mesh.

Figure 2.12 shows the corresponding pressure f elds at the nodes for the nodal-based tetrahedron. This solution uses the stabilization parameters $\alpha = 0.005$ and $\beta = 0.01$. A f rst observation is that the pressure ranges vary widely, and are very different from the hexahedral solutions. The

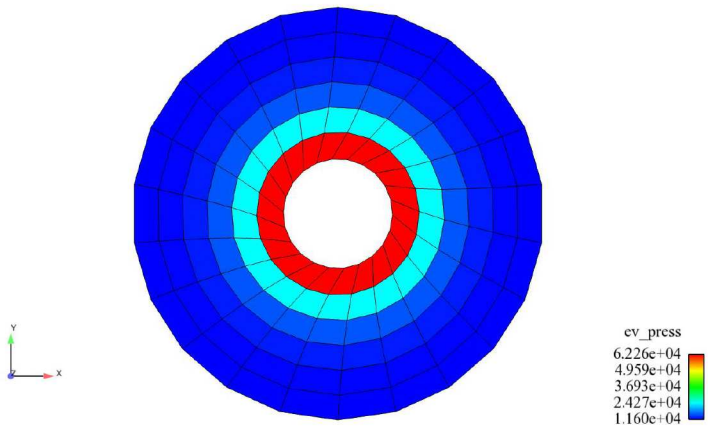

(a) Coarse Mesh: 7 elements in radial direction

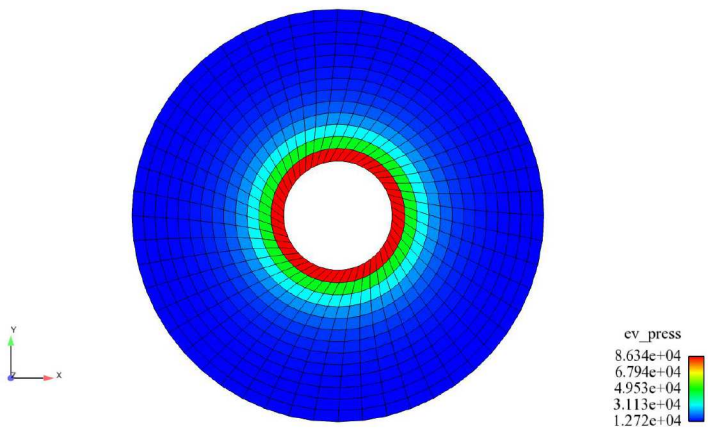

(b) Medium Mesh: 13 elements in radial direction

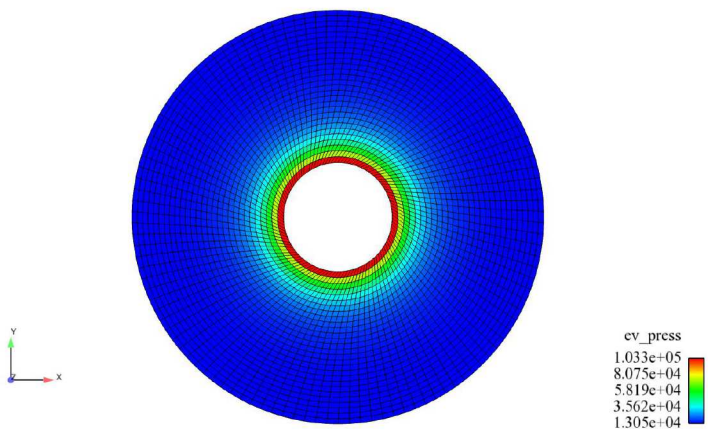

(c) Fine Mesh: 28 elements in radial direction

Figure 2.10. Pressure prof les for elastic shear problem with regularly meshed hexes. Pressure prof les in each picture cover the minimum and maximum range of pressures in the analysis.

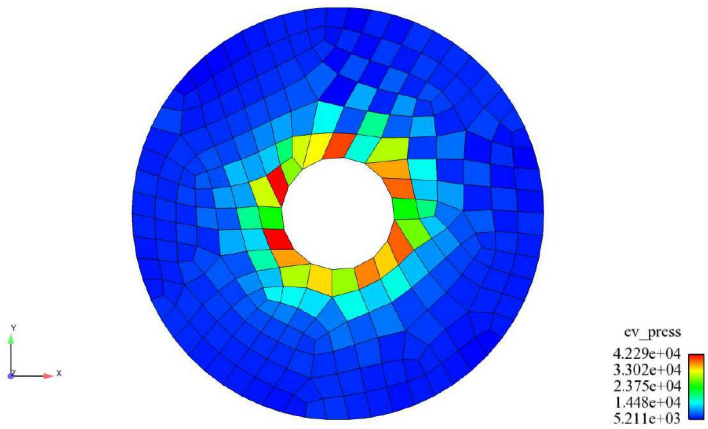

(a) Coarse Mesh: 7 elements in radial direction

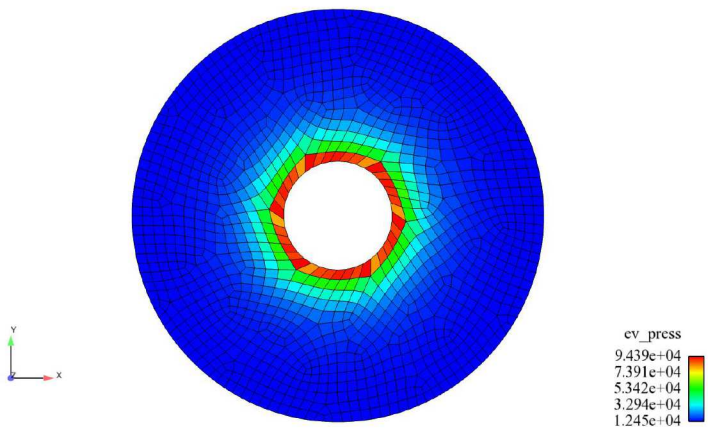

(b) Medium Mesh: 13 elements in radial direction

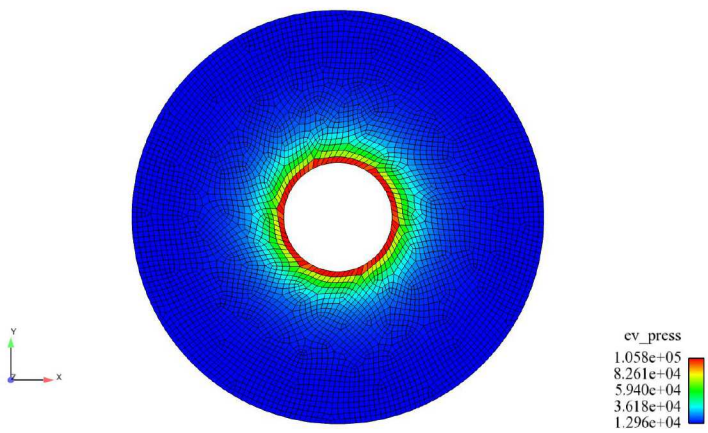

(c) Fine Mesh: 28 elements in radial direction

Figure 2.11. Pressure prof les for elastic shear problem with paved hex meshes. Pressure prof les in each picture cover the minimum and maximum range of pressures in the analysis.

solution also deviates from expectation by not being constant in the angular direction. In each case, the pressure ranges include negative as well as positive pressures, whereas the hex mesh only had positive values. In the fine hex case, pressures ranged from 1.3e+4 to 1.0e+5, but for the finest nodal-base tet case, the pressures range from -5.9e+5 to 4.4e+5. The solutions also do not look smooth, and appear to have isolated spots of high pressure. This variation is more clearly shown in Figure 2.13. These are the same results as in the previous figure, but with pressure contours limited to range from -1.0e+4 to 1.0e+4. What is apparent from these plots is that the pressures vary widely in a fairly random fashion, even between adjacent nodes. This also does not appear to be alleviated with mesh refinement.

Figure 2.14 shows the deformation on the inner radius for the finest mesh. Pressure fields in this diagram range from 0.0 to 1.0e5. Clearly, the pressure fields vary wildly and violate the expected (and, at least from the hex case, demonstrated) smoothness of solution. A close investigation of this figure gives a clue to the cause of the variation of the pressure field. The pressure differences appear to roughly correspond with changes in the mesh connectivity. Connectivity changes are visible in the figure as a change in the orientation of the diagonals used to convert the hexes into tets. For instance, a dark blue band visible along the inner radius is clearly a region of zero or negative pressure. This band also happens to correspond to a region where the diagonals are opposed – they form a chevron. In the other parts of the inner radius, the diagonals are generally aligned, and the corresponding pressures are positive. Close inpection of the previous pressure plots with the nodal-based tets for this problem show the same kind of pattern; stress concentrations change at or near a change in connectivity. This issue will become even more evident in the next example problem – a cylinder in torsion.

All of the results shown previously are for one selection of the stabilization parameters, $\alpha = 0.005$ and $\beta = 0.01$. The effect of varying these parameters is shown in Figure 2.15. The solution is strongly affected by the selection of parameters, yet in no case are the pressure solutions completely smooth. There are always locations where adjacent nodes show variation that seems to violate the symmetry of the problem.

Furthermore, just looking at one surface may not show the largest variation of pressure. In Figure 2.16, the pressure solution on the front and back of a nodal-based tetrahedral analysis with $\alpha = 0.01, \beta = 0.6$ is shown. The back shows a significantly larger variation in pressure than the front side.

Investigation of the individual stress components for the coarse mesh gives additional insight into the mechanisms that drive the pressure issues for the nodal-based tet. Figures 2.17 and 2.18 show σ_{xx}, σ_{yy}, and σ_{zz}; the sum of these terms divided by 3 is the pressure. For both the nodal and element stabilization terms, the σ_{xx} and σ_{yy} appear to be fairly well-behaved; the values look reasonably smooth and symmetric (though there is definitely an observable affect of the mesh). However, σ_{zz} mirrors the pressure solution, although it's overall magnitude is significantly less than the other terms.

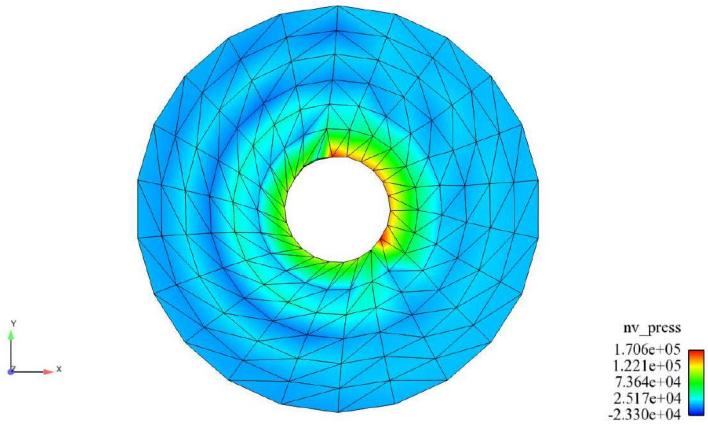

(a) Coarse Mesh: 7 elements in radial direction

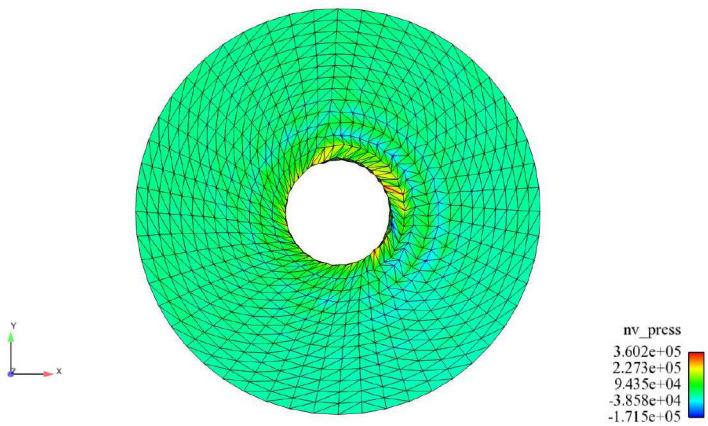

(b) Medium Mesh: 13 elements in radial direction

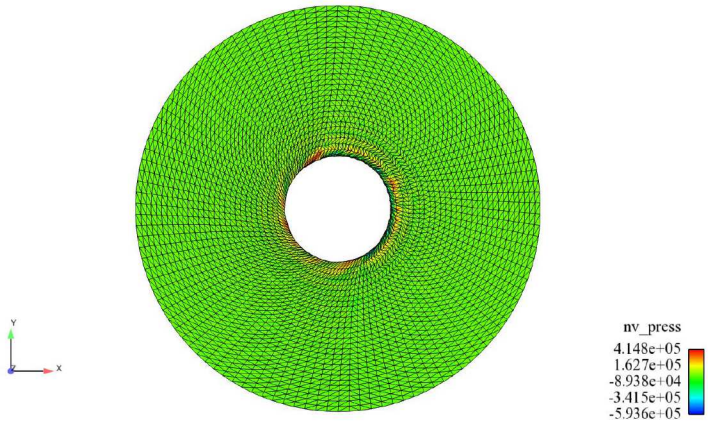

(c) Fine Mesh: 28 elements in radial direction

Figure 2.12. Pressure prof les for elastic shear problem with nodal-based tets created from hex meshes. Pressure prof les in each picture cover the minimum and maximum range of pressures in the analysis. Note the ever-increasing range of pressures, which are both positive and negative.

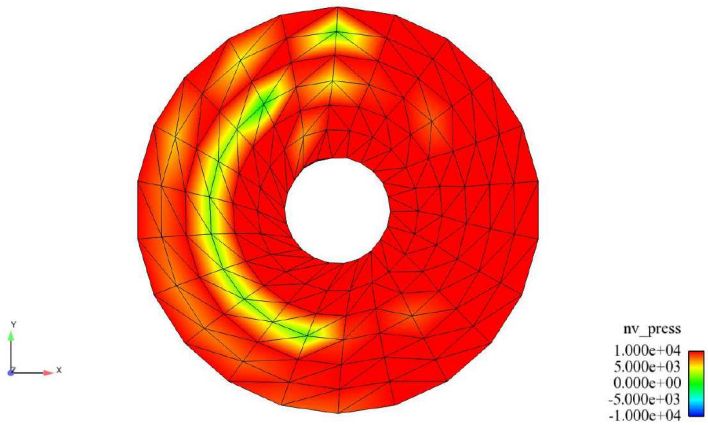

(a) Coarse Mesh: 7 elements in radial direction

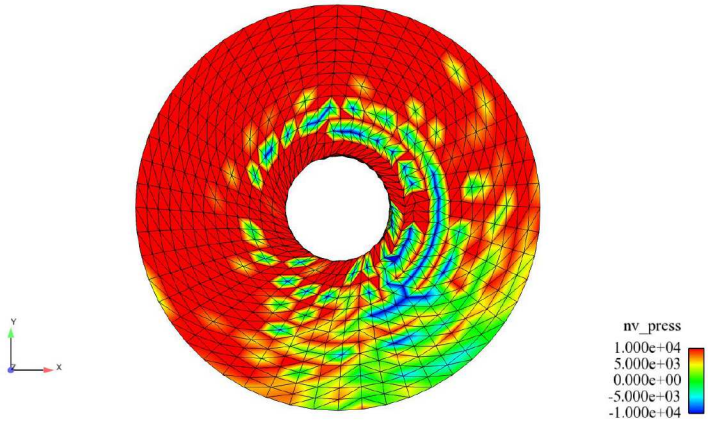

(b) Medium Mesh: 13 elements in radial direction

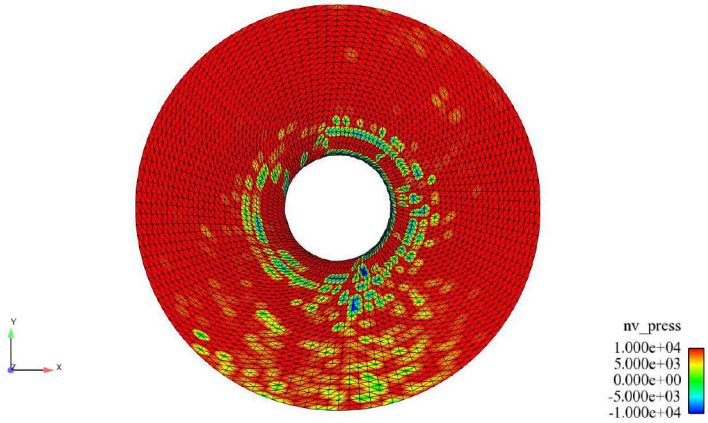

(c) Fine Mesh: 28 elements in radial direction

Figure 2.13. Pressure prof les for elastic shear problem with nodal-based tets created from hex meshes. Pressure prof les in each picture cover from 1e4 to -1e4. Nodes that are adjacent on the mesh may have opposite signs, even in the ref ned mesh.

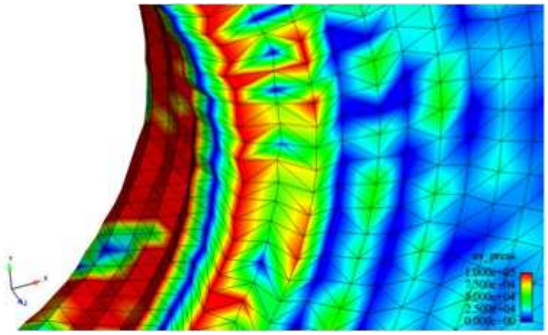

Figure 2.14. Pressures and uneven deformation of inner radius on f ne mesh for nodal-based tet solution, $\alpha = 0.005$ and $\beta = 0.01$.

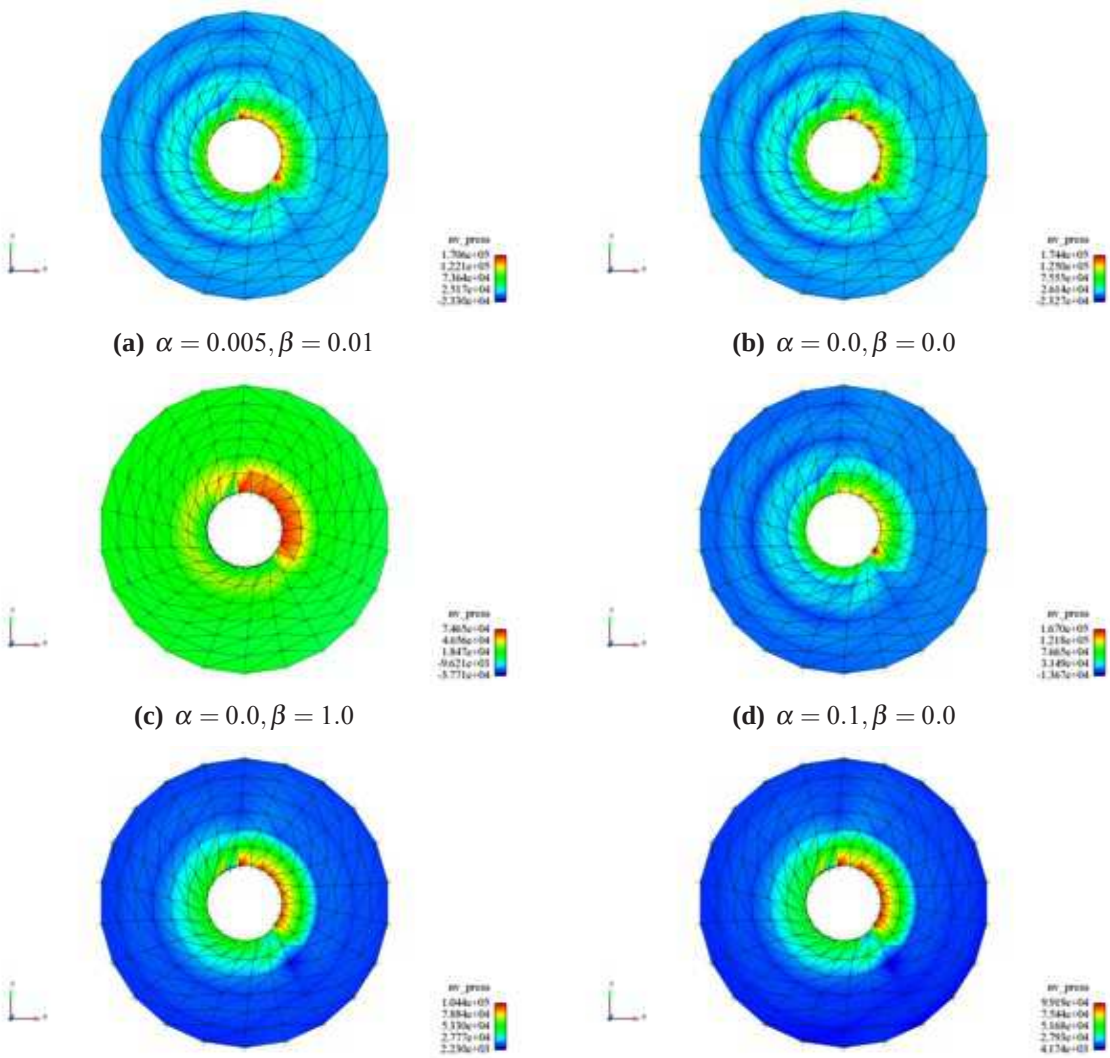

(a) $\alpha = 0.005, \beta = 0.01$

(b) $\alpha = 0.0, \beta = 0.0$

(c) $\alpha = 0.0, \beta = 1.0$

(d) $\alpha = 0.1, \beta = 0.0$

(e) $\alpha = 0.01, \beta = 0.35$ (default)

(f) $\alpha = 0.1, \beta = 0.35$

Figure 2.15. Pressure solutions for coarse nodal-based tetrahedral mesh for various values of α and β.

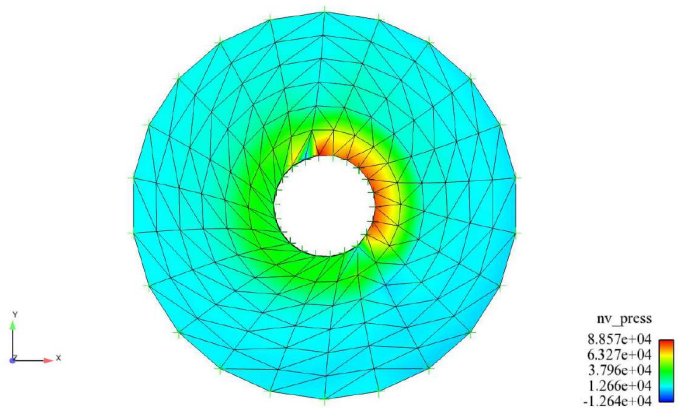

(a) $\alpha = 0.01, \beta = 0.6$, front

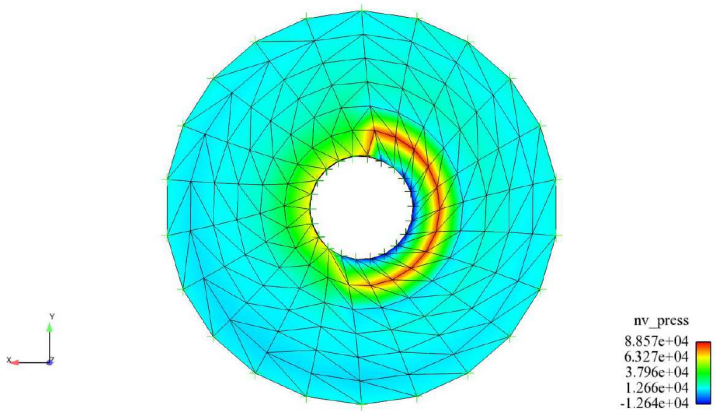

(b) $\alpha = 0.01, \beta = 0.6$, back

Figure 2.16. Pressure solution for front and back of coarse nodal-based tetrahedral mesh with $\alpha = 0.01$ and $\beta = 0.6$.

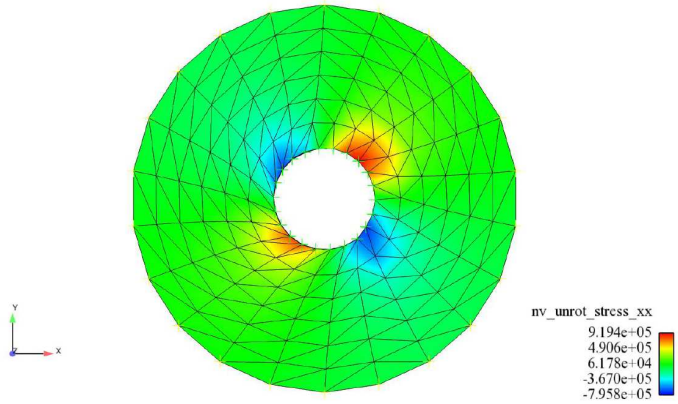

(a) Nodal stress solution, σ_{xx} component

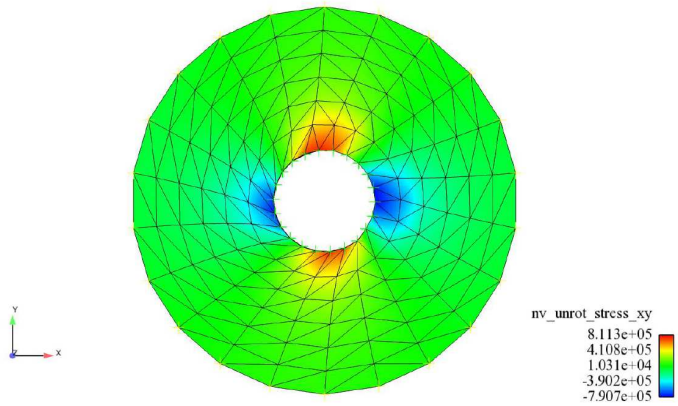

(b) Nodal stress solution, σ_{yy} component

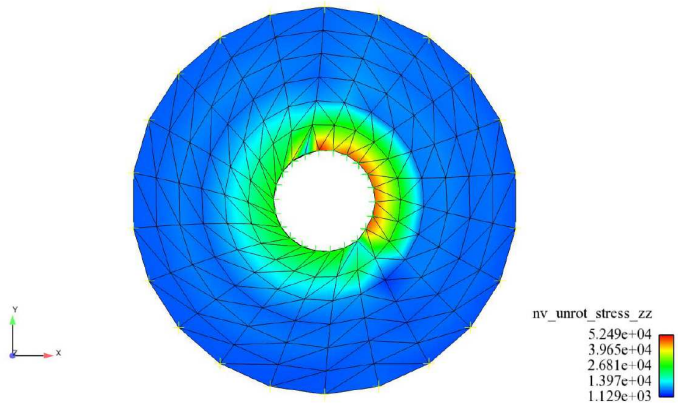

(c) Nodal stress solution, σ_{zz} component

Figure 2.17. Stress components for nodal solution of coarse mesh.

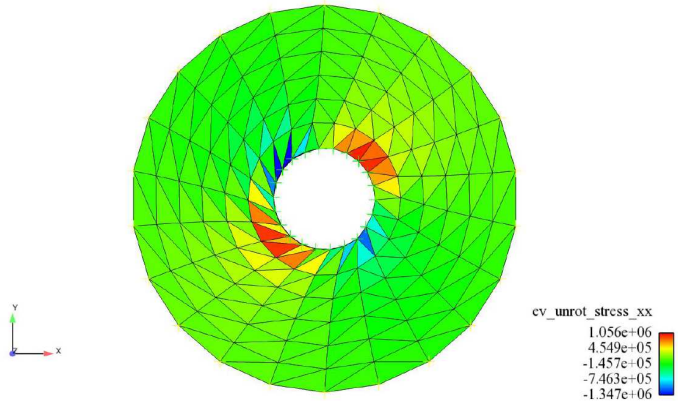

(a) Element stress solution, σ_{xx} component

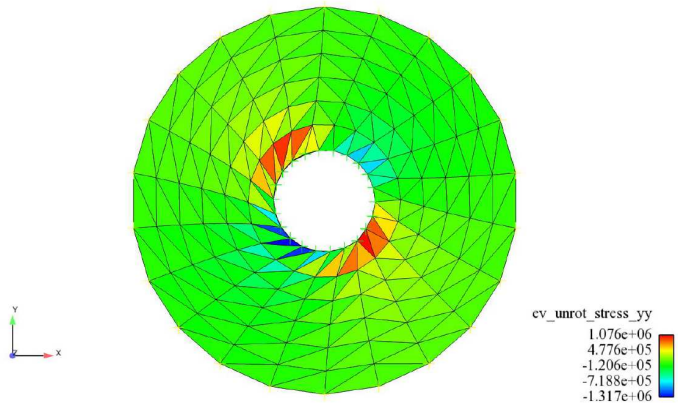

(b) Element stress solution, σ_{yy} component

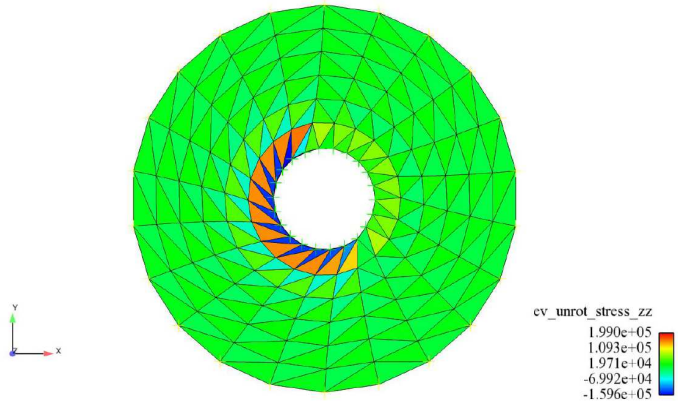

(c) Element stress solution, σ_{zz} component

Figure 2.18. Stress components for nodal solution of coarse mesh.

Torsional Cylinder

The final example problem is a cylinder, 2 units high and 2 units in diameter, subjected to a torsional loading. The exterior of the cylinder is unconstrained, the bottom is free to move in the radial direction but is fixed in the tangential direction (i.e. no rotation around the center axis), and the top has a prescribed displacement tangential to the axis but is free in the radial direction. The displacement of the top corresponds to a .14 radian (8 degree) rotation around the central axis of the cylinder. The cylinder is allowed to contract along it's length. An elastic material is used with a Youngs modulus of 100.0 and Poissons ratio of 0.25.

This problem was meshed four ways: hexes, nodal-based tets converted from the hex mesh using 6 tets per hex, nodal-based tets paved from the original cylindrical geometry, and nodal-based tets using the "cross-triangle" technique (meshed from hexes using 24 tets per hex). The ability to create a cross-triangle mesh using a base hex mesh is a brand new capability in the ENCORE module in Sierra, and enables comparison to codes that use the cross-trangle formulation extensively, such as EPIC [8]. In each of these meshes, three levels of mesh refinement were made, with 4, 8, and 24 elements through the radius for the coarse, medium, and fine meshes, respectively.

Figure 2.19 shows the pressure fields for the hex meshes. As the mesh is refined, the solution looks more and more symmetric, with a positive pressure on the outside, and a negative pressure on the inside. The pressure range for the finest mesh ranges from -0.0469 to 0.0244. The results from the nodal-based tet mesh converted from hexes using 6 tets per hex is shown in Figure 2.20, while the results from the nodal-based tet with a paved mesh is shown in Figure 2.21. In both of these cases, the pressure solutions show significant variation, with pressure "hot-spots" spread around the surface of the mesh. The maximum and minimum pressure values are two to three times higher in magnitude than those seen on the hex mesh: -0.114 to .0613 on the converted mesh and -0.0746 to 0.0689 on the paved mesh. On the meshes converted from hexes, pressure concentrations seem to be particulary sensitive to changes in the connectivity of the elements; if the diagonals switch direction or don't all meet at a node in the same way as adjacent elements, then the node is likely to have a pressure concentration. This problem does not go away with mesh refinement; if anything, it appears to get worse. Figure 2.22 shows results on the finest mesh converted from hexes, both on the outside of the cylinder and also along a cut in the middle of the cylinder. These plots clearly indicate that the pressure concentrations do not just occur at the top surface; they extend all throughout the solution, and a general oscillatory pressure field appears to be present.

Figure 2.23 shows the pressure fields for the nodal-based tets using the cross-triangle mesh for each level of refinement. Even at the coarsest level, these results compare favorably to the hex results. The pressures are not perfectly uniform; it is clear that the pressures are a little different where the nodes lie at the center versus the vertex of the original hexes. However, the uniformity of solution looks very good, and continues to get better with mesh refinement. It should be noted that using standard tets with this cross-triangle mesh does not yield a solution with the same quality as the nodal-based tet. Figure 2.24 shows the pressure profiles on a cut plane through the center of the cylinder on the coarsest cross-triangle mesh. The standard tet solution shows large pressure oscillations in adjoining elements, while the nodal-based tet shows a smooth solution as we would expect.

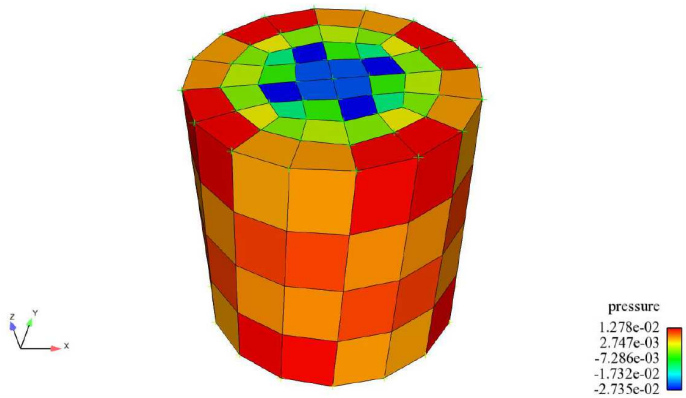

(a) Hex mesh, coarse resolution

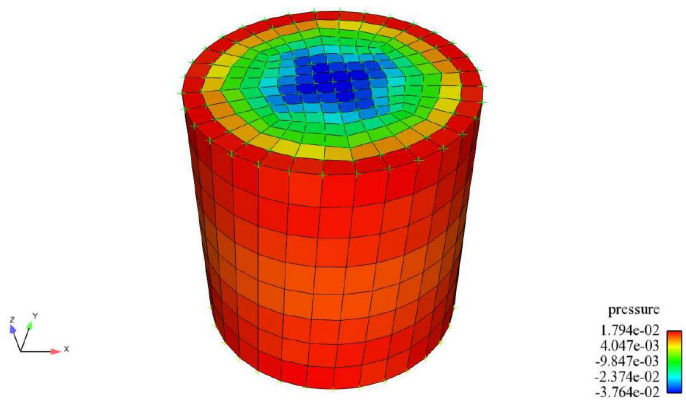

(b) Hex mesh, medium resolution

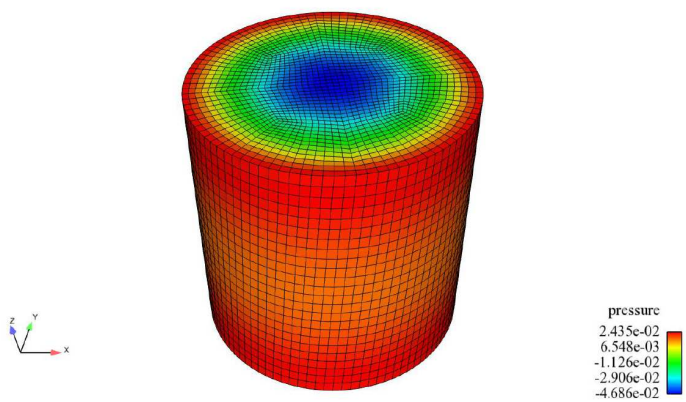

(c) Hex mesh, f ne resolution

Figure 2.19. Pressures in torsional cylinder using a hex mesh.

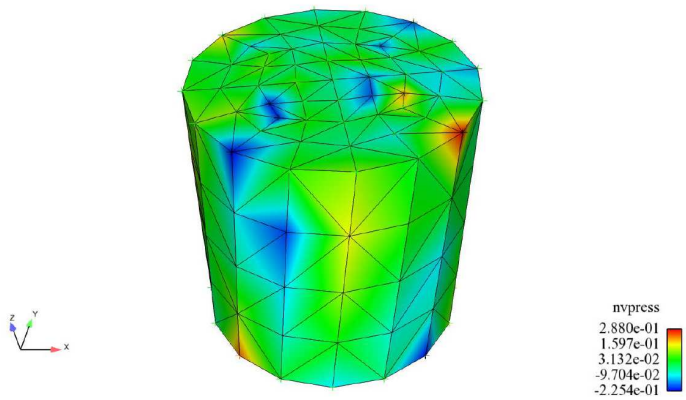

(a) Nodal-based tet mesh from hex, coarse resolution

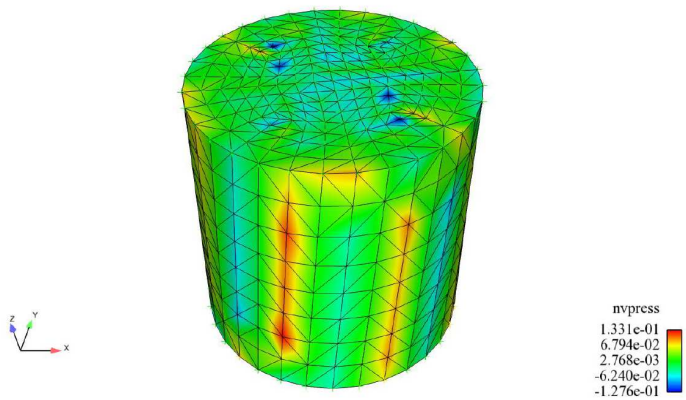

(b) Nodal-based tet mesh from hex, medium resolution

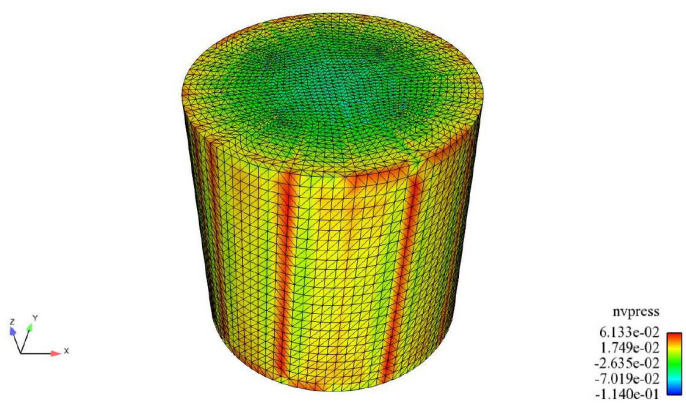

(c) Nodal-based tet mesh from hex, f ne resolution

Figure 2.20. Pressures in torsional cylinder using a nodal-based tet mesh generated from corresponding hex mesh.

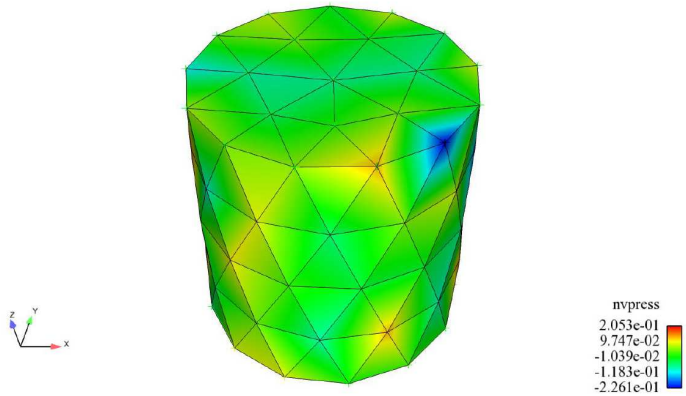

(a) Paved nodal-based tet mesh, coarse resolution

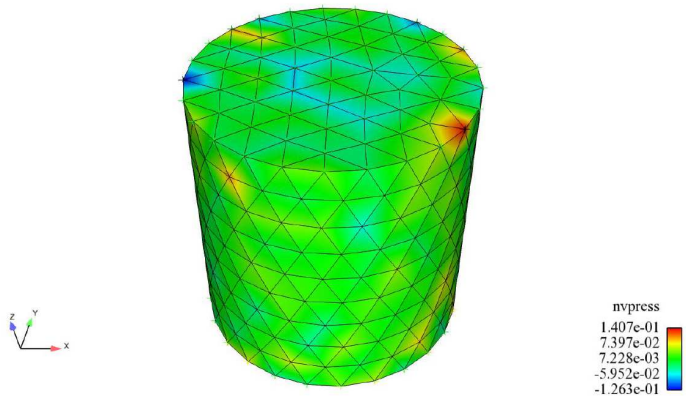

(b) Paved nodal-based tet mesh, medium resolution

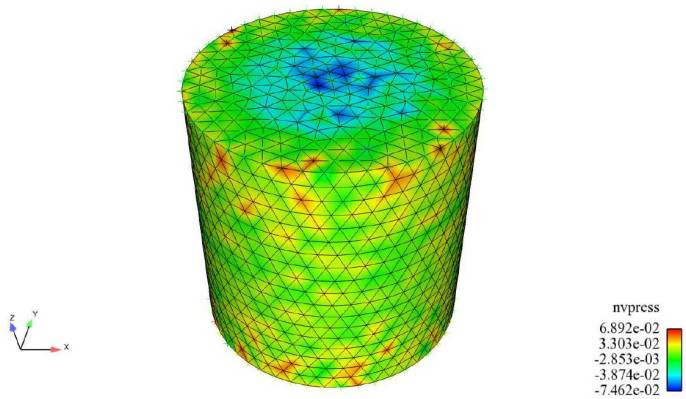

(c) Paved nodal-based tet mesh, f ne resolution

Figure 2.21. Pressures in torsional cylinder using a paved nodal-based tet mesh.

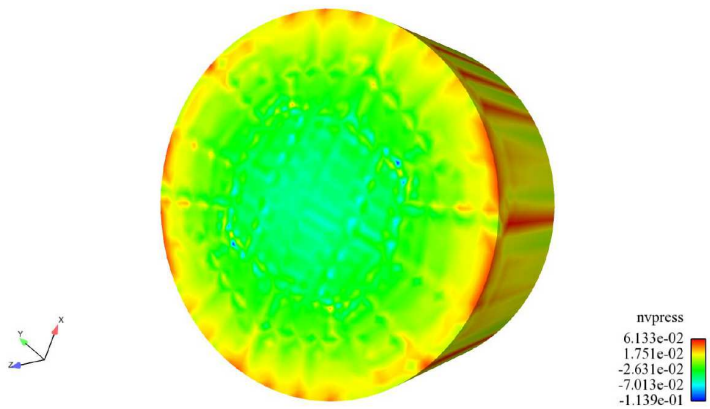

(a) Pressures on top surface of f nest nodal-based tet mesh

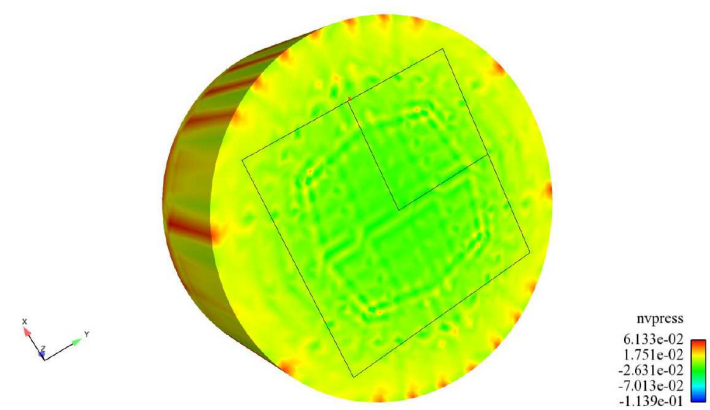

(b) Pressures on cut through middle of f nest nodal-based tet mesh

Figure 2.22. Pressures on exterior/interior of f nest nodal-based tet mesh.

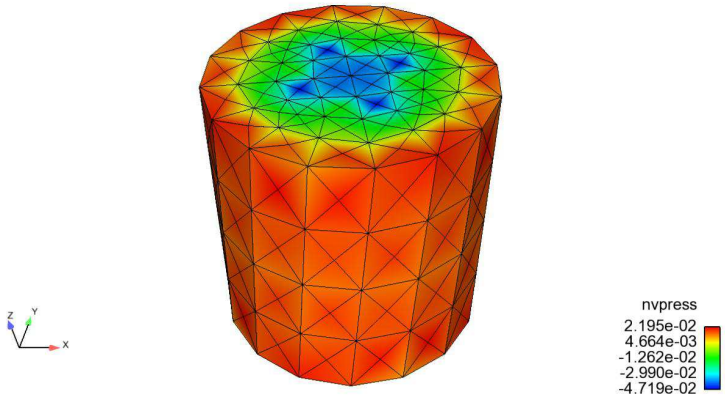

(a) Cross-triangle nodal-based tet mesh, coarse resolution

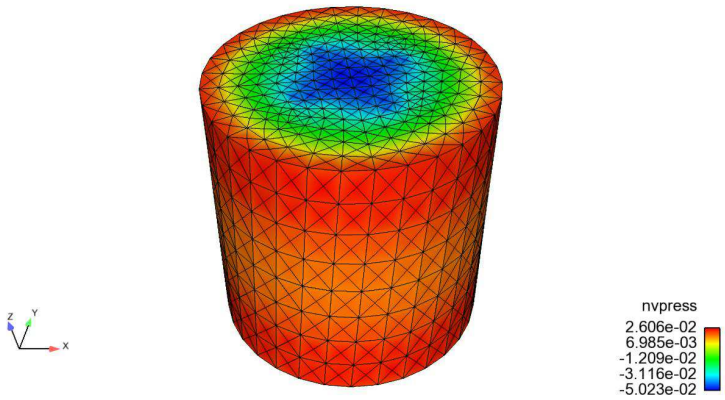

(b) Cross-triangle nodal-based tet mesh, medium resolution

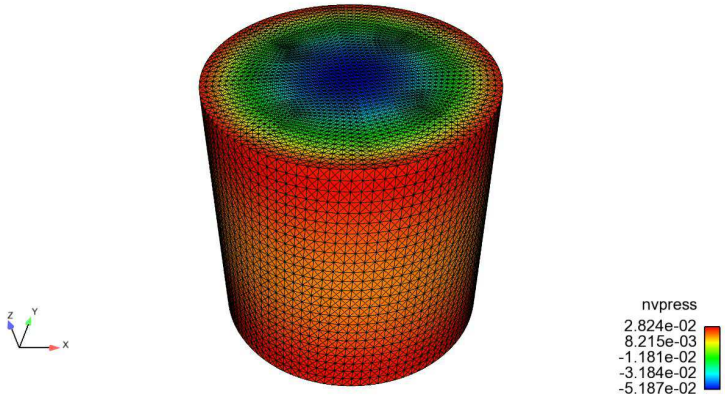

(c) Cross-triangle nodal-based tet mesh, f ne resolution

Figure 2.23. Pressures in torsional cylinder using a cross-triangle nodal-based tet mesh (24 tets per hex).

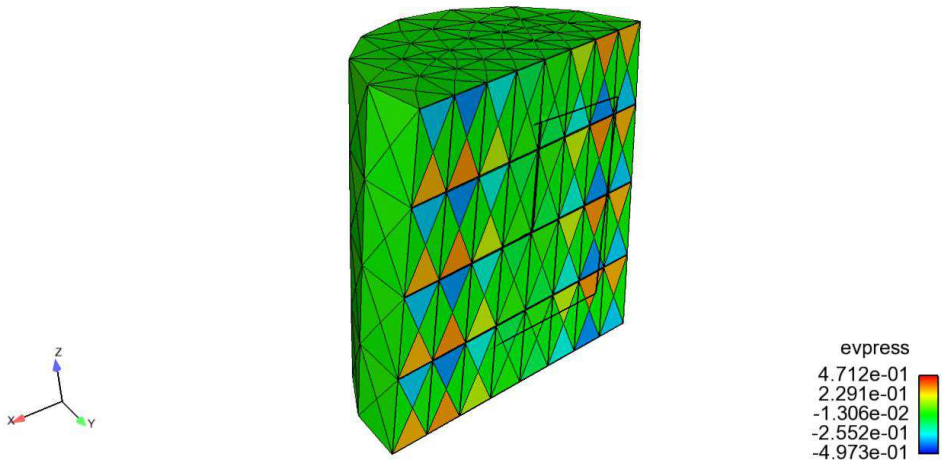

(a) Cross-triangle mesh, standard 4-node tet

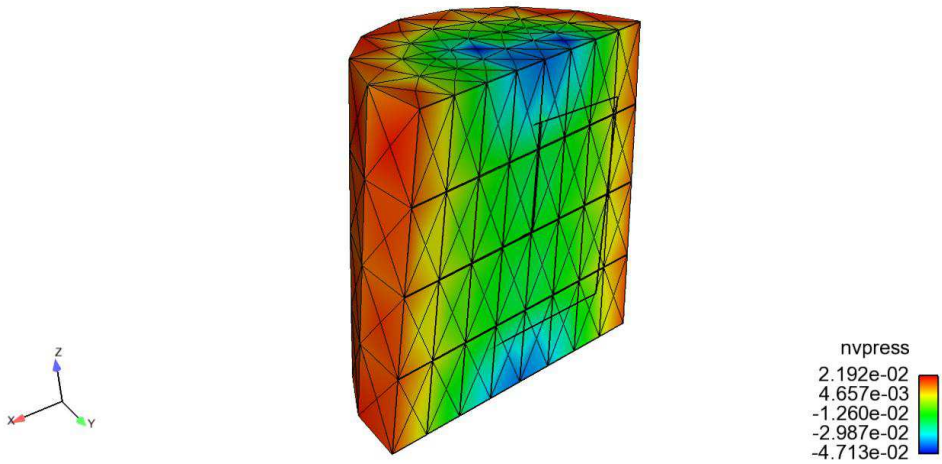

(b) Cross-triangle mesh, nodal-based tet

Figure 2.24. Pressures through center of cylinder with cross-triangle mesh, with standard and nodal-based tets.

Chapter 3

Conclusions

The previous section detailed six sets of analyses that explored the behavior of the nodal-based tetrahedron (tet). The analyses were run in the explicit transient-dynamics mode of the Sierra/SM code, but in general with a smooth load function designed to approximate quasi-static loading. In most cases, an elastic material was used to simplify the element assessments. In each case, the nodal-based tet solution was compared to a solution from uniform-gradient hex elements. Various metrics for comparison were used to assess the overall behavior of the elements, but the primary metric was the quality of the pressure f eld. For materials that have a strong dependence on pressure, such as equation-of-state materials, the quality of the pressure f eld is vital for accurate consitutive response.

In a number of these problems, the nodal-based tet elements produced solutions with global metrics that matched theoretical or experimental results. The elements passed the patch test, produced qualitatively good solutions for the Cook's membrane test, computed accurate tip displacements for beam bending, and provided reasonable displacement metrics for the Taylor bar impact.

Despite these successes, the nodal-based tet elements appear to produce a poor quality pressure f eld, especially when the solution is primarily driven in shear. Even though the nodal-based tets provided reasonable global results on the beam bending and Taylor bar impact cases, the pressure f elds were not as smooth as expected, and varied substantially more than solutions from equivalent hex meshes. The pressure f elds for the elastic shear and torsion cylinder cases were very poor, and the solutions did not improve with mesh ref nement. Varying the stabilization parameters (α and β), or even turning them off altogether, did not remove the problems. The one approach that did seem to alleviate these problems was to use the nodal-based tets in a "cross-triangle" formulation, where a hex mesh is converted to tets using 24 tets per hex. This is quite expensive, but appears to give a smooth result.

The exact cause of these problems with the nodal-based tet is still uncertain, but the results of these problems seem to indicate a high dependence on nodal connectivity. Sudden changes in pressure appear to correspond to locations where the local connectivity changes, be it a change in direction of the diagonals across a converted hex element or a change in the number of elements that meet at a node in a paved mesh. The success of cross-triangle meshes further illustrates the effect of mesh connectivity – constraining the mesh to have a very regular connectivity at each node enables the nodal-based tet to give what appears to be a good quality solution. A more conclusive proof of why connectivity matters so much in nodal-based tets should be achievable using small

patches of elements with varying connectivity, but these were not able to be completed by the end of this project.

These conclusions have a strong impact on the use of the nodal-based tet. The Cook's membrane test may suggest that a material that experiences signif cant plasticity and is subjected to limited shear can still produce a good quality answer when using these elements. The global metrics for various other problems (Taylor bar impact and beam bending) also looked reasonable. However, even when the global metrics appear to be good, the pressure f eld at the nodes may be poor. If the material model being used is dependent on the pressure f eld (e.g. equation-of-state models), then these elements as currently implemented are a poor choice. A better pressure f eld can be achieved using a cross-triangle mesh, but this requires the creation of an original hex mesh f rst and will generally be many times more expensive computationally than the original hex mesh.

The remeshing capability for nodal-based tets also must be used with care. One of the primary advantages of the nodal-based tet is that material state variables are caried primarily at the nodes. When coupled with a remeshing strategy that seeks to preserve nodal locations, the level of mapping required after a remesh step is minimized. However, if the solution is highly dependent on the connectivity of the mesh, then the remeshed geometry can have very different behavior than the parent mesh, even though the node locations are preserved. This can lead to instabilities. The elastic shear problem, for instance, tends to become unstable once remeshing is turned on. Furthermore, when a new node is added during remeshing, it's values are copied from the closest pre-existing node. If the solution f eld has a high level of variability (as it does in pressure), then the values it copies may be very different depending on which node it is closest to. This can result in very different solutions due to small roundoff differences in relative location. It should be noted that problems dominated by plastic f ow and with little shear, such as the case of Cook's membrane, may function just f ne with remeshing. For instance, the elastic shear problem run with an elastic-nearly-prefectly-plastic material is typically stable with remeshing.

Further investigation into the behavior of the nodal-based tet is recommended. Although this report contains a variety of problems that point out def ciencies in its behavior, it does not provide a conclusive demonstration of the cause of these problems. Although not reported in this report, additional work has been attempted in creating smaller patch-like meshes that can be more thouroughly analyzed to identify why connectivity matters so much for this element. Current results have been inconclusive, but further work will likely yield insights that may help point towards remedies for this behavior. It is possible that code bugs still exist that are causing these issues, but if they exist, they are not obvious given the good quality of certain aspects of the solution. Another option for future investigation is the creation of a mixed formulation, where the pressures are also included degrees of freedom. This has shown signif cant promise in other work [11], and may have applicability here. In the mean time, the nodal-based tets should be used with substantial caution.

References

[1] N. Crane. Nodal based tetrahedrons and remeshing for modeling of extreme loadings on underground structures. In *79th Shock and Vibration Symposium*, Orlando, FL, October 2008.

[2] N. Crane. Nodal Based Tets and Remeshing. Technical Report SAND2008-7091P, Sandia National Laboratories, Sandia National Laboratories, Albuquerque, NM, 2008.

[3] N. Crane, A. Gullerud, D. Littlewood, and A. Lindblad. Comparison of computational fracture techniques for dynamic tensile extrusion test. In *10th Annual United States National Conference on Computaionatial Mechanics*, Columbus, OH, July 2009.

[4] C. Dohrmann, M. Heinstein, J. Jung, S. W. Key, and W. Witkowski. Node-based uniform strain elements for three-node triangular and four-node tetrahedral meshes. *International Journal For Numerical Methods in Engineering*, 47:1549–1568, 2000.

[5] M. W. Gee, C. R. Dohrmann, S. W. Key, and W. A. Wall. A uniform nodal strain tetrahedron with isochoric stabilization. *International Journal For Numerical Methods in Engineering*, 78:429–443, 2009.

[6] T. Hughes. *The Finite Element Method: Linear Static and Dynamic Finite Element Analysis*. Dover Publications Inc., Mineola, NY, 2000.

[7] B. M. Irons and A. Razzaque. Experiences with the patch test for convergence of f nite elements. In A. K. Aziz, editor, *The Mathematical Foundations of the Finite Element Method with Applications to Partial Differential Equations*, pages 557–587, New York, NY, 1972. Academic Press.

[8] G. R. Johnson, S. R. Beissel, C. A. Gerlach, R. A. Stryk, T. J. Holmquist, A. A. Johnson, S. E. Ray, and J. J. Arata. User Instructions for the 2006 Version of the EPIC Code. Final Report for US Army Research Laboratory Contact DAAD19-03-D-0001, Network Computing Services, P.O. Box 581459, Minneapolis, MN 55458, 2006.

[9] S. Key, J. Gruda, M. Heinstein, A. Gullerud, N. Crane, and C. Dohrmann. A Performance Comparison of Three Finite Elements For Used in Transient Dynamics Simulations. Unpublished work, March 2005.

[10] M. Puso and J. Solberg. A stabilized nodally integrated tetrahedral. *International Journal For Numerical Methods in Engineering*, 67:841–867, 2006.

[11] G. Scovazzi, M. A. Christon, T. J. R. Hughes, and J. N. Shadid. Stabilized shock hydrodynamics: I. a lagrangian method. *Computer Methods in Applied Mechanics and Engineering*, 196:923–966, 2007.

[12] SIERRA Solid Mechanics Team. Presto 4.16 User's Guide. Technical Report SAND2010-3112, Sandia National Laboratories, Sandia National Laboratories, Albuquerque, NM, 2010.

DISTRIBUTION:

1	MS 0380	Joe Jung, 01542
1	MS 0380	Martin Heinstein, 01542
1	MS 0380	Nathan Crane, 01542
1	MS 0380	Jason Hales, 01542
1	MS 0380	Sam Key, 01542
1	MS 0380	Kyran Mish, 01542
1	MS 0380	Kendall Pierson, 01542
1	MS 0380	Vicki Porter, 01542
1	MS 0380	Tim Shelton, 01542
1	MS 0380	Ben Spencer, 01542
1	MS 0380	Jessie Thomas, 01542
1	MS 1322	Dave Littlewood, 01435
1	MS 0372	Bill Scherzinger, 01524
1	MS 0372	Nicole Breivik, 01524
1	MS 0372	Ken Gwinn, 01542
1	MS 0372	Edmundo Corona, 01542
1	MS 0372	Jeff Gruda, 01525
1	MS 0372	Jim Redmond, 01525
1	MS 0847	Steve Attaway, 01525
1	MS 0372	Kristin Dion, 01525
1	MS 0372	Jerry Wellman, 01525
1	MS 0372	Jake Ostien, 08246
1	MS 9042	Jay Foulk, 08246
1	MS 9042	Aljandro Mota, 08246
1	MS 9042	Jay Dike, 08249
		,
1	MS 0899	Technical Library, 9536 (electronic copy)
1	MS 0123	D. Chavez, LDRD Off ce, 1011

Sandia National Laboratories